This is a peer-reviewed, author's accepted manuscript of the following research article: Abad, F., Rouzegar, J., & Lotfian, S. (2023).
Application of the exact spectral element method in the analysis of the smart functionally graded plate.
Steel and Composite Structures, 47(2), 297-313.
https://doi.org/10.12989/scs.2023.47.2.297

Application of the exact spectral element method in the analysis of the smart functionally graded plate

Farhad Abad*[1,2], Jafar Rouzegar[1a] and Saeid Lotfian[2b]

[1] *Department of Mechanical and Aerospace Engineering, Shiraz University of Technology, Shiraz, PO Box-71555-313, Iran.*
[2] *Department of Naval Architecture, Ocean and Marine Engineering, University of Strathclyde, Glasgow G4 0LZ, UK.*

(Received keep as blank , Revised keep as blank , Accepted keep as blank)

Abstract. This study aims to extend the application of the spectral element method (SEM) to wave propagation and free vibration analysis of functionally graded (FG) plates integrated with thin piezoelectric layers, plates with tapered thickness and structure on elastic foundations. Also, the dynamic response of the smart FG plate under impact and moving loads is presented. In this paper, the dynamic stiffness matrix of the smart rectangular FG plate is determined by using the exact dynamic shape functions based on Mindlin plate assumptions. The low computational time and results' independence with the number of elements are two significant features of the SEM. Also, to prove the accuracy and efficiency of the SEM, results are compared with Abaqus simulations and those reported in references. Furthermore, the effects of boundary conditions, power-law index, piezoelectric layers thickness, and type of loading on the results are studied.

Keywords: Wave propagation; Spectral Element Method; Tapered thickness; Elastic foundation; Piezoelectric layer; Moving load

1. Introduction

Studies on the different structures, including piezoelectric layers, have increased in the recent decade. Electro-mechanical coupling, large power generation, high-frequency response and vacuum capability of piezoelectric materials made them widely employed in engineering purposes, like automobile industries, construction, computers and even orthopaedic usages (Kulkarni et al. 2018; Taherifar et al. 2020; Liu et al. 2022; Panda et al. 2022). Functionally graded (FG) structures have many outstanding properties compared to traditional materials, such as excellent heat resistance, high wear resistance, high stiffness, and long fatigue life (Koizumi 1993). Although combining FG plates with piezoelectric layers increases their applications, it also leads to more complex behaviour and the structure's response due to electro-mechanical coupling (Martínez-Ayuso et al. 2019). A significant number of numerical and analytical methods have been presented for analyzing the smart FG structures in different conditions (Ebrahimi and Barati 2016; Ebrahimi and Barati 2018; Ahmed et al. 2021; Tran et al. 2023). Lv et al. (2019) presented the Piezoelectric Element Differential Method, a new numerical method for simulating the electro-mechanical behaviour of piezoelectric structures with FGM properties. Through solving various examples, they demonstrated the accuracy of the presented method. Fenjan, Ahmed et al. (2020) presented the static stability buckling characteristics of quasi-3D piezo-magnetic functional grading nanoplates. Also, Fenjan, Ahmed et al. (2021) investigated the nonlinear thermal buckling behaviour of a nano-sized beam with piezo-magnetic properties, including geometrical imperfection. They studied the effect of electrical voltage, piezoelectric constituent volume and magnetic potential on buckling temperatures. Jiang et al. (2021) proposed the Zonal Free Element Method (ZFREM) handle piezoelectric structures with intricate shapes. They put the method to the test by solving multiple two-dimensional (2D) and three-dimensional (3D) problems and were able to overcome challenges posed by corners by incorporating a mapping technique. Liu et al. (2021) investigated wave propagation analysis of small-scaled functionally graded piezoelectric (FGP) plates based on modified couple stress theory and proved that their presented formulation has high computational efficiency and good convergence. Fazeli et al. (2021) studied the vibration response of stepped cross-ply laminated composite beams with piezoelectric layers in different configurations and validated their results using finite element modelling and experiments. Abbaspour and Arvin (2021) applied the Ritz method based on FSDT for buckling analysis of nanocomposite microplates resting on an elastic foundation. They studied the effects of temperature, voltage, power-law index, and angular velocity of the structure under different loading conditions. Al-Osta (2022) presented the wave propagation analysis in porous FG plates subjected to hygrothermal environments using first-order shear deformation theory (FSDT). They also studied the effect of temperatures and moisture on the power law parameter of the FG plate. Mirjavadi, Forsat et al. (2022) studied the nonlinear free vibrations of stiffened porous FG annular spherical shell segments. They considered two types of porosity distributions, including the effect of

*Corresponding author, Ph.D.,
E-mail: farhad.abad@strath.ac.uk
[a]Associate Professor
E-mail: rouzegar@sutech.ac.ir
[b]Ph.D., Research Fellow
E-mail: saeid.lotfian@strath.ac.uk

stiffeners and the surrounding medium, and proposed an analytical method to solve the nonlinear governing equations.

The spectral element method (SEM) is an almost new family of numerical methods whose basic concepts are introduced by Narayanan and Beskos (1978). The SEM is a frequency domain method; therefore, the first step in this method is transforming the differential equations of motion into the frequency domain using the Discrete Fourier Transform (DFT). The second step is determining the shape functions of the structure by solving the dispersion equation, and then the structure's dynamic stiffness matrix (DSM) is formulated. Attaining the exact results by using the least number of elements, performing the time and frequency domain analysis, and independence of the results to the number of elements (Lee 2009; Khalili et al. 2017) are some unique advantages of the SEM which make it an attractive method for wave propagation and dynamic analysis of various structures (Nanda and Kapuria 2015; Azandariani et al. 2022; Kulkarni et al. 2022). Liu 2016; Liu et al. (2016) have developed the SEM for modal and dynamic response analysis of a composite plate with different boundary conditions, non-uniform support, mass attachments, and elastic coupling constraints. They also solved a wide range of examples to manifest the applicability of the SEM for composite structures. Joglekar and Mitra (2016) have conducted the SEM for the wave propagation analysis of a cracked beam. They solved several examples and compared the SEM results with the finite element simulations to prove the method's capability. Furthermore, they presented a parametric study to investigate the effect of different kinds of cracks on the results. Mokhtari et al. (2017) have applied SEM for vibration analysis of a moving pre-tensioned beam. They presented a new technique to solve the partial differential equations and compared the SEM results with the finite element analyses. Abad and Rouzegar (2017) have developed the SEM for free vibration analysis of Levy-type smart FG plates with piezoelectric layers. They studied the effect of various parameters on the structure's natural frequencies, such as piezoelectric layers, FG plate thicknesses, and boundary conditions. Also, they developed the SEM for the dynamic response of smart isotropic plates under impact loading and introduced a new efficient and accurate algorithm to calculate the structure's natural frequencies (Abad and Rouzegar 2019).

Though there are several studies on the dynamic analysis of smart plates by different analytical and numerical methods and the SEM has been employed for various analyses of plate structures, to the authors' knowledge, there is no study on the application of the SEM on dynamic analysis and wave propagation of smart FG plates. This research attempts to develop a spectral element formulation for wave propagation analysis of a Levy-type FG plate with two piezoelectric layers bonded to its surfaces under the action of moving and impact loadings. Additionally, various critical examples are solved to prove the application of the SEM method, such as plates with tapered thickness and the structure on elastic foundations. The results are compared with those obtained from Abaqus simulations and other existing solutions. Also, the effect of type of boundary conditions, piezoelectric layers thickness, power-law index and kind and amount of loading on the dynamic response of the smart FG plate is studied.

2. Theoretical Formulation

Figure 1 illustrates a rectangular FG plate with a thickness of $2h$ and length a, width b (in x and y directions), which is integrated with two thin piezoelectric layers (with the thickness of h_p). x and y are the in-plane coordinates, and z is in the normal direction of the Cartesian system, which is in the corner of the mid-plane of the structure. In this paper, the Levy-type boundary condition is considered for the structure; accordingly, edges located along x=0 and x=a are simply supported.

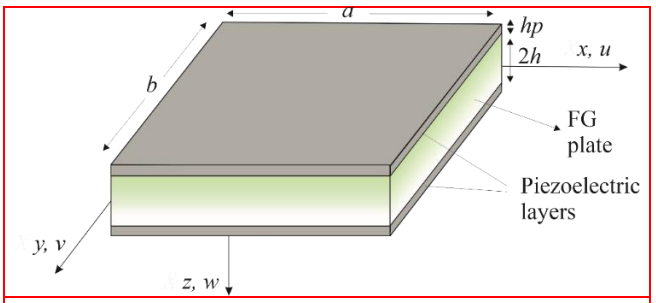

Fig. 1 A schematic view of the FG plate integrated with two piezoelectric layers at the top and bottom surfaces.

2.1 Governing equations

Considering the Mindlin plate theory assumptions, the displacement field of the smart FG plate is written as:

$$\begin{Bmatrix} u(x,y,z) \\ v(x,y,z) \\ w(x,y,z) \end{Bmatrix} = \begin{Bmatrix} u_0(x,y,t) \\ v_0(x,y,t) \\ w_0(x,y,t) \end{Bmatrix} + z \begin{Bmatrix} \psi_x(x,y,t) \\ \psi_y(x,y,t) \\ 0 \end{Bmatrix} \quad (1)$$

where u_0, v_0, w_0, ψ_x and ψ_y are five displacement components placed on the mid-plane of the base plate. The strain-displacement relationships are given by:

$$\begin{Bmatrix} \varepsilon_{xx} \\ \varepsilon_{yy} \\ \gamma_{xy} \end{Bmatrix} = \varepsilon_0 + z\kappa_0, \begin{Bmatrix} \gamma_{xz} \\ \gamma_{yz} \end{Bmatrix} = \gamma_0 \quad (2)$$

where

$$\varepsilon_0 = \begin{Bmatrix} \frac{\partial u_0}{\partial x} \\ \frac{\partial v_0}{\partial y} \\ \frac{\partial u_0}{\partial y} + \frac{\partial v_0}{\partial x} \end{Bmatrix}, \kappa_0 = \begin{Bmatrix} \frac{\partial \psi_x}{\partial x} \\ \frac{\partial \psi_y}{\partial y} \\ \frac{\partial \psi_x}{\partial y} + \frac{\partial \psi_y}{\partial x} \end{Bmatrix}, \gamma_0 = \begin{Bmatrix} \psi_x + \frac{\partial w_0}{\partial x} \\ \psi_y + \frac{\partial w_0}{\partial y} \end{Bmatrix} \quad (3)$$

The constitutive relations for the piezoelectric layers, which couple the electric and elastic fields, are expressed by:

Application of the exact spectral element method in the analysis of the smart functionally graded plate

$$\begin{Bmatrix}\sigma_{xx}\\ \sigma_{yy}\\ \sigma_{xy}\\ \sigma_{xz}\\ \sigma_{yz}\end{Bmatrix}=\begin{bmatrix}\bar{C}_{11} & \bar{C}_{12} & 0 & 0 & 0\\ \bar{C}_{12} & \bar{C}_{11} & 0 & 0 & 0\\ 0 & 0 & \frac{1}{2}(\bar{C}_{11}-\bar{C}_{12}) & 0 & 0\\ 0 & 0 & 0 & C_{55} & 0\\ 0 & 0 & 0 & 0 & C_{55}\end{bmatrix}\begin{Bmatrix}\varepsilon_{xx}\\ \varepsilon_{yy}\\ \gamma_{xy}\\ \gamma_{xz}\\ \gamma_{yz}\end{Bmatrix}-\begin{bmatrix}0 & 0 & \bar{e}_{31}\\ 0 & 0 & \bar{e}_{31}\\ 0 & 0 & 0\\ -e_{51} & 0 & 0\\ 0 & -e_{51} & 0\end{bmatrix}\begin{Bmatrix}E_x\\ E_y\\ E_z\end{Bmatrix} \quad (4)$$

$$\begin{Bmatrix}D_x\\ D_y\\ D_z\end{Bmatrix}=\begin{bmatrix}0 & 0 & 0 & e_{51} & 0\\ 0 & 0 & 0 & 0 & e_{51}\\ \bar{e}_{31} & \bar{e}_{31} & 0 & 0 & 0\end{bmatrix}\begin{Bmatrix}\varepsilon_{xx}\\ \varepsilon_{yy}\\ \gamma_{xy}\\ \gamma_{xz}\\ \gamma_{yz}\end{Bmatrix}+\begin{bmatrix}\Xi_{11} & 0 & 0\\ 0 & \Xi_{11} & 0\\ 0 & 0 & \bar{\Xi}_{33}\end{bmatrix}\begin{Bmatrix}E_x\\ E_y\\ E_z\end{Bmatrix} \quad (5)$$

$$\phi(x,y,z,t)=\begin{cases}\varphi(x,y,t)\left[1-\left(\dfrac{z-h-\frac{h_p}{2}}{\frac{h_p}{2}}\right)^2\right], h\le z\le h+h_p\\ \varphi(x,y,t)\left[1-\left(\dfrac{-z-h-\frac{h_p}{2}}{\frac{h_p}{2}}\right)^2\right], -h-h_p\le z\le -h\end{cases} \quad (10)$$

where $\bar{C}_{11}$ to $\bar{C}_{55}$ and $\bar{e}_{31}$ to $\bar{e}_{51}$ are the stiffness coefficients and piezoelectric constants, respectively, as introduced in Appendix A. E and D are the electric field intensity and electric displacement vector, Ξ is the dielectric constant matrix and ε, and σ are the strain and stress tensors. The constitutive relation for the FG plate is defined as:

$$\begin{Bmatrix}\sigma_{xx}\\ \sigma_{yy}\\ \sigma_{xy}\\ \sigma_{xz}\\ \sigma_{yz}\end{Bmatrix}=\begin{bmatrix}Q_{11} & Q_{12} & 0 & 0 & 0\\ Q_{12} & Q_{11} & 0 & 0 & 0\\ 0 & 0 & Q_{44} & 0 & 0\\ 0 & 0 & 0 & Q_{55} & 0\\ 0 & 0 & 0 & 0 & Q_{66}\end{bmatrix}\begin{Bmatrix}\varepsilon_{xx}\\ \varepsilon_{yy}\\ \gamma_{xy}\\ \gamma_{xz}\\ \gamma_{yz}\end{Bmatrix} \quad (6)$$

in which the coefficients Q_{ij} can be written as

$$Q_{11}=Q_{22}=\frac{E(z)}{1-\nu^2}$$
$$Q_{12}=\frac{\nu E(z)}{1-\nu^2} \quad (7)$$
$$Q_{44}=Q_{55}=Q_{66}=\frac{E(z)}{2(1+\nu)}$$

Material properties of the FG plate are considered to vary smoothly over the thickness based on the following power-law equation:

$$E(z)=E_m+(E_c-E_m)\left(\frac{1}{2}-\frac{z}{2h}\right)^n,$$
$$\rho(z)=\rho_m+(\rho_c-\rho_m)\left(\frac{1}{2}-\frac{z}{2h}\right)^n \quad (8)$$

In which n is the power-law index and subscripts c and m denote the characteristic of ceramic and metal parts, respectively. In Eq. (8), n=0 and n=∞ represents a fully ceramic and metal structure. According to the following relation, the electric field E is obtained from the electrostatic potential ϕ:

$$E_i=-\phi_{,i}\quad i=1,2,3 \quad (9)$$

In this paper, zero voltage condition is considered for the surfaces of piezoelectric layers; accordingly, the electrostatic potential is defined as (Rouzegar and Abad 2015):

Hamilton's principle is employed for extracting the equations of motion of the smart FG plate.

$$\int_0^t(\delta U+\delta V-\delta T)\,dt=0 \quad (11)$$

where δ indicates the variation of parameters and V, T, and U are the work done by the applied loading, kinetic and strain energy, respectively.

$$\delta V=-\int_x\int_y(f(x,y,t)\delta w)dydx \quad (12)$$

$$\delta T=\rho\int_x\int_y\int_z(\dot{u}\delta\dot{u}+\dot{v}\delta\dot{v}+\dot{w}\delta\dot{w})\,dzdydx \quad (13)$$

$$\delta U=\int_x\int_y\int_z\big(\sigma_{xx}\delta\varepsilon_{xx}+\sigma_{yy}\delta\varepsilon_{yy}+\tau_{xy}\delta\gamma_{xy}+\kappa\tau_{xz}\delta\gamma_{xz}+\kappa\tau_{yz}\delta\gamma_{yz}\big)\,dzdydx \quad (14)$$

where κ is the shear correction factor, and $f(x,y,t)$ is the applied force in the z-direction. Regarding five independent variations (u_0, v_0, w_0, ψ_x and ψ_y), equations of motion are derived:

$$\begin{aligned}\delta u_0&: N_{xx,x}+N_{xy,y}=I_0\ddot{u}_0+I_1\ddot{\psi}_x\\ \delta v_0&: N_{xy,x}+N_{yy,y}=I_0\ddot{v}_0+I_1\ddot{\psi}_y\\ \delta\psi_x&: M_{xx,x}+M_{xy,y}-Q_x=I_1\ddot{u}_0+I_2\ddot{\psi}_x+c_0\dot{\psi}_x\\ \delta\psi_y&: M_{yy,y}+M_{xy,y}-Q_y=I_1\ddot{v}_0+I_2\ddot{\psi}_y+c_0\dot{\psi}_y\\ \delta w&: Q_{x,x}+Q_{y,y}=I_0\ddot{w}+c_0\dot{w}\end{aligned} \quad (15)$$

The following damping coefficient, which is related to the mean value of mass density, damping ratio (ξ), and fundamental natural frequency, is added to Eq. (15) to modify the inertia terms (Lee 2009; Shirmohammadi, Bahrami et al. 2015):

$$c_0=2\rho\omega_1\xi \quad (16)$$

In which stress resultants and inertias of the structure are defined in Eq. (17).

$$\begin{gathered}(N_{xx}, N_{yy}, N_{xy}) = \int_{-h-h_p}^{h+h_p} (\sigma_x, \sigma_y, \sigma_{xy}) dz, \\ (I_i) = \int_{-h-h_p}^{h+h_p} \rho z^i dz\,, \\ (M_{xx}, M_{yy}, M_{xy}) = \int_{-h-h_p}^{h+h_p} (\sigma_x, \sigma_y, \sigma_{xy}) z dz, \\ (Q_{yz}, Q_{xz}) = \int_{-h-h_p}^{h+h_p} (\sigma_{yz}, \sigma_{xz}) dz\end{gathered} \quad (17)$$

By substituting Eqs. (1-4) and (17) into Eq. (15), the differential equations are obtained in terms of displacements components:

$$A_{11}(u_{0,xx} + v_{0,xy}) + A_{66}(u_{0,yy} - v_{0,xy}) + B_{11}(\psi_{x,xx} + \psi_{y,xy}) + B_{66}(\psi_{x,yy} - \psi_{y,xy}) = I_0\ddot{u}_0 + I_1\ddot{\psi}_x \quad (18a)$$

$$A_{11}(u_{0,xy} + v_{0,yy}) - A_{66}(u_{0,xy} - v_{0,xx}) + B_{11}(\psi_{x,xy} + \psi_{y,yy}) - B_{66}(\psi_{x,xy} - \psi_{y,xx}) = I_0\ddot{v}_0 + I_1\ddot{\psi}_y \quad (18b)$$

$$B_{11}(u_{0,xx} + v_{0,xy}) + B_{66}(u_{0,yy} - v_{0,xy}) - A_{55}(w_{,x} + \psi_x) + F_{11}(\psi_{x,xx} + \psi_{y,xy}) + F_{66}(\psi_{x,yy} - \psi_{y,xy}) + (\lambda_2 - \lambda_1)\varphi_{,x} = I_1\ddot{u}_0 + I_2\ddot{\psi}_x + c_0\dot{\psi}_x \quad (18c)$$

$$B_{11}(u_{0,xy} + v_{0,yy}) - B_{66}(u_{0,xy} - v_{0,xx}) - A_{55}(w_{,y} + \psi_y) + F_{11}(\psi_{x,xy} + \psi_{y,yy}) - F_{66}(\psi_{x,xy} - \psi_{y,xx}) + (\lambda_2 - \lambda_1)\varphi_{,x} = I_1\ddot{v}_0 + I_2\ddot{\psi}_y + c_0\dot{\psi}_y \quad (18d)$$

$$A_{55}(w_{,xx} + w_{,yy} + \psi_{x,x} + \psi_{y,y}) - \lambda_2(\varphi_{,xx} + \varphi_{,yy}) + f(x,y,t) = I_0\ddot{w} + c_0\dot{w} \quad (18e)$$

In which the coefficients A_{ij}, B_{ij}, F_{ij} are the structure stiffness, and λ_i are introduced in Appendix A. The potential electric field of the piezoelectric layer can be achieved by considering the integral form of Maxwell's equation:

$$\int_h^{h+h_p} \vec{\nabla} \cdot \vec{D}\, dz + \int_{-h-h_p}^{-h} \vec{\nabla} \cdot \vec{D}\, dz = 0 \quad (19)$$

Substituting Eqs. (1-5) and (9-10), into Eq. (19) yields:

$$\lambda_3\nabla^2 w + \lambda_2\nabla^2\varphi + \lambda_4(\psi_{x,x} + \psi_{y,y}) + \lambda_5\varphi = 0 \quad (20)$$

By applying the Discrete Fourier Transform (DFT) theory, equations (18) and (20), which are the time domain illustration of differential equations, can be transformed into the frequency domain. The spectral form of the displacement and electrostatic potential components are:

$$\begin{Bmatrix} u_0(x,y,t) \\ v_0(x,y,t) \\ \psi_x(x,y,t) \\ \psi_y(x,y,t) \\ w(x,y,t) \\ \varphi(x,y,t) \end{Bmatrix} = \sum_{n=1}^{N} \begin{Bmatrix} \bar{u}_{0,n}(x,y;\omega_n) \\ \bar{v}_{0,n}(x,y;\omega_n) \\ \bar{\psi}_{x,n}(x,y;\omega_n) \\ \bar{\psi}_{y,n}(x,y;\omega_n) \\ \bar{w}_n(x,y;\omega_n) \\ \bar{\varphi}_n(x,y;\omega_n) \end{Bmatrix} exp(i\omega_n t) \quad (21)$$

Also, the spectral form of the external force is:

$$f(x,y,t) = \sum_{n=1}^{N} \bar{F}(x,y;\omega_n)\, exp(i\omega_n t) \quad (22)$$

In which N is the number of time samples. Accurate results in the Fourier transform depend on the sample time; accordingly, several parameters should be considered for choosing a proper value for N (Newland 2012). For briefness, the indexes n will be neglected in the subsequent relations. Substituting Eq. (21) into Eqs. (18) and (20) lead to the frequency domain representation of differential equations:

$$A_{11}(\bar{u}_{0,xx} + \bar{v}_{0,xy}) + A_{66}(\bar{u}_{0,yy} - \bar{v}_{0,xy}) + B_{11}(\bar{\psi}_{x,xx} + \bar{\psi}_{y,xy}) + B_{66}(\bar{\psi}_{x,yy} - \bar{\psi}_{y,xy}) + I_0\omega^2\bar{u}_0 + I_1\omega^2\bar{\psi}_x = 0 \quad (23a)$$

$$A_{11}(\bar{u}_{0,xy} + \bar{v}_{0,yy}) - A_{66}(\bar{u}_{0,xy} - \bar{v}_{0,xx}) + B_{11}(\bar{\psi}_{x,xy} + \bar{\psi}_{y,yy}) - B_{66}(\bar{\psi}_{x,xy} - \bar{\psi}_{y,xx}) + I_0\omega^2\bar{v}_0 + I_1\omega^2\bar{\psi}_y = 0 \quad (23b)$$

$$B_{11}(\bar{u}_{0,xx} + \bar{v}_{0,xy}) + B_{66}(\bar{u}_{0,yy} - \bar{v}_{0,xy}) - A_{55}(\bar{w}_{,x} + \bar{\psi}_x) + F_{11}(\bar{\psi}_{x,xx} + \bar{\psi}_{y,xy}) + F_{66}(\bar{\psi}_{x,yy} - \bar{\psi}_{y,xy}) + (\lambda_2 - \lambda_1)\bar{\varphi}_{,x} + I_1\omega^2\bar{u}_0 + (I_2\omega^2 - ic_0\omega)\bar{\psi}_x = 0 \quad (23c)$$

$$B_{11}(\bar{u}_{0,xy} + \bar{v}_{0,yy}) - B_{66}(\bar{u}_{0,xy} - \bar{v}_{0,xx}) + F_{11}(\bar{\psi}_{x,xy} + \bar{\psi}_{y,yy}) - F_{66}(\bar{\psi}_{x,xy} - \bar{\psi}_{y,xx}) - A_{55}(\bar{w}_{,y} + \bar{\psi}_y) + (\lambda_2 - \lambda_1)\bar{\varphi}_{,x} + I_1\omega^2\bar{v}_0 + (I_2\omega^2 - ic_0\omega)\bar{\psi}_y = 0 \quad (23d)$$

$$A_{55}(\bar{w}_{,xx} + \bar{w}_{,yy} + \bar{\psi}_{x,x} + \bar{\psi}_{y,y}) - \lambda_2(\bar{\varphi}_{,xx} + \bar{\varphi}_{,yy}) + \bar{F}(x,y) + (I_0\omega^2 - ic_0\omega)\bar{w} = 0 \quad (23e)$$

$$\lambda_2(\nabla^2\bar{w} - \nabla^2\bar{\varphi}) + \lambda_3(\bar{\psi}_{x,x} + \bar{\psi}_{y,y}) + \lambda_4\bar{\varphi} = 0 \quad (23f)$$

2.2 Exact Dynamic Shape Functions

Application of the exact spectral element method in the analysis of the smart functionally graded plate

$$\bar{u}_{0n}(x,y;\omega_n)=\sum_{m=1}^{\infty} c\cos\left(\frac{m\pi}{a}x\right)exp(-iky),\bar{v}_{0n}(x,y;\omega_n)=\sum_{m=1}^{\infty} r_1^m c\sin\left(\frac{m\pi}{a}x\right)exp(-iky)$$
$$\bar{\psi}_{xn}(x,y;\omega_n)=\sum_{m=1}^{\infty} r_2^m c\cos\left(\frac{m\pi}{a}x\right)exp(-iky),\bar{\psi}_{yn}(x,y;\omega_n)=\sum_{m=1}^{\infty} r_3^m c\sin\left(\frac{m\pi}{a}x\right)exp(-iky) \quad (24)$$
$$\bar{w}_n(x,y;\omega_n)=\sum_{m=1}^{\infty} r_4^m c\sin\left(\frac{m\pi}{a}x\right)exp(-iky),\bar{\varphi}_n(x,y;\omega_n)=\sum_{m=1}^{\infty} r_5^m c\sin\left(\frac{m\pi}{a}x\right)exp(-iky)$$

In order to form the exact dynamic shape functions of the differential equation, it is required to build and solve the dispersion equation. The series presented in Eq. (24) are defined for displacement and electrostatic potential components, where *m* and *k* represent wave and mode numbers. By substituting Eq. (24) into the homogenous form (setting $\bar{F}(x,y)=0$) of Eq. (23), the following eigenvalue problem is obtained for the rectangular Levy-type smart FG plate:

$$\begin{bmatrix} z_{11} & z_{12} & z_{13} & z_{14} & z_{15} & z_{16} \\ z_{21} & z_{22} & z_{23} & z_{24} & z_{25} & z_{26} \\ z_{31} & z_{32} & z_{33} & z_{34} & z_{35} & z_{36} \\ z_{41} & z_{42} & z_{43} & z_{44} & z_{45} & z_{46} \\ z_{51} & z_{52} & z_{53} & z_{54} & z_{55} & z_{56} \\ z_{61} & z_{62} & z_{63} & z_{64} & z_{65} & z_{66} \end{bmatrix} \begin{Bmatrix} 1 \\ r_1 \\ r_2 \\ r_3 \\ r_4 \\ r_5 \end{Bmatrix} c = 0 \quad (25)$$

In which the components of matrix *z* are defined in Appendix B. Setting the determinant of the coefficient matrix equal to zero, a 12th-order dispersion equation is achieved:

$$k^{12}+d_1k^{10}+d_2k^8+d_3k^6+d_4k^4+d_5k^2+d_6=0 \quad (26)$$

edges *y*=0 and *y*=*b*, constant vectors (c_q) will be determined. It worth noting that on these edges, piezoelectric layers are electrically insulated (Farsangi et al. 2013):

2.3 Dynamic stiffness matrix

There are several methods to formulate the Dynamic Stiffness Matrix (DSM). The force-displacement method is the most convenient one, which obtains the DSM by relating nodal displacements and force vectors (Szilard 2004). The values of the spectral form of displacement, electrostatic potential, and stress resultants on two edges of the element are as below (Eqs. 30 and 31):

$$\begin{aligned} \bar{u}_{01}&=\bar{u}_0(x,0;\omega), & \bar{u}_{02}&=\bar{u}_0(x,b;\omega), \\ \bar{v}_{01}&=\bar{v}_0(x,0;\omega), & \bar{v}_{02}&=\bar{v}_0(x,b;\omega), \\ \bar{\psi}_{x1}&=\bar{\psi}_x(x,0;\omega), & \bar{\psi}_{x2}&=\bar{\psi}_x(x,b;\omega), \\ \bar{\psi}_{y1}&=\bar{\psi}_y(x,0;\omega), & \bar{\psi}_{y2}&=\bar{\psi}_y(x,b;\omega), \\ \bar{w}_1&=\bar{w}(x,0;\omega), & \bar{w}_2&=\bar{w}(x,b;\omega), \\ \bar{\varphi}_1&=\bar{\varphi}(x,0;\omega), & \bar{\varphi}_2&=\bar{\varphi}(x,b;\omega) \end{aligned} \quad (30)$$

$$\bar{u}_{0n}(x,y;\omega_n)=\sum_{m=1}^{\infty}\sum_{q=1}^{12}\cos\left(\frac{m\pi}{a}x\right)c_q\,exp(-ik_qy)=\sum_{m=1}^{\infty}\cos\left(\frac{m\pi}{a}x\right)\hat{e}(y,\omega)c^T$$
$$\bar{v}_{0n}(x,y;\omega_n)=\sum_{m=1}^{\infty}\sum_{q=1}^{12}\sin\left(\frac{m\pi}{a}x\right)r_{1q}^m c_q\,exp(-ik_qy)=\sum_{m=1}^{\infty}\sin\left(\frac{m\pi}{a}x\right)R_1\hat{e}(y,\omega)c^T$$
$$\bar{\psi}_{xn}(x,y;\omega_n)=\sum_{m=1}^{\infty}\sum_{q=1}^{12}\cos\left(\frac{m\pi}{a}x\right)r_{2q}^m c_q\,exp(-ik_qy)=\sum_{m=1}^{\infty}\cos\left(\frac{m\pi}{a}x\right)R_2\hat{e}(y,\omega)c^T$$
$$\bar{\psi}_{yn}(x,y;\omega_n)=\sum_{m=1}^{\infty}\sum_{q=1}^{12}\sin\left(\frac{m\pi}{a}x\right)r_{3q}^m c_q\,exp(-ik_qy)=\sum_{m=1}^{\infty}\sin\left(\frac{m\pi}{a}x\right)R_3\hat{e}(y,\omega)c^T \quad (27)$$
$$\bar{w}_n(x,y;\omega_n)=\sum_{m=1}^{\infty}\sum_{q=1}^{12}\sin\left(\frac{m\pi}{a}x\right)r_{4q}^m c_q\,exp(-ik_qy)=\sum_{m=1}^{\infty}\sin\left(\frac{m\pi}{a}x\right)R_4\hat{e}(y,\omega)c^T$$
$$\bar{\varphi}_n(x,y;\omega_n)=\sum_{m=1}^{\infty}\sum_{q=1}^{12}\sin\left(\frac{m\pi}{a}x\right)r_{5q}^m c_q\,exp(-ik_qy)=\sum_{m=1}^{\infty}\sin\left(\frac{m\pi}{a}x\right)R_5\hat{e}(y,\omega)c^T$$

where

$$\hat{e}(y,\omega)=\{exp(-ik_1y)\quad exp(-ik_2y)\quad exp(-ik_3y)\ldots\quad exp(-ik_{12}y)\}$$
$$c=\{c_1\quad c_2\quad c_3\ldots\quad c_{12}\} \quad (28)$$
$$R_p(\omega)=diag\left[r_{pq}^m\right],(p=1,2,3,4,5;q=1,2,3,\ldots,12)$$

$$at\ y=0,b\rightarrow\begin{cases} either\ \varphi(x,y,t)|_{y=0,b}=0 \\ or\ \int_h^{h+h_p}D_z(x,y,z,t)|_{y=0,b}\,dz+\int_{-h-h_p}^{-h}D_z(x,y,z,t)|_{y=0,b}\,dz=0 \end{cases} \quad (29)$$

By solving the dispersion equation, twelve wave numbers k_q (q=1, 2, 3, …, 12) and five eigenvectors r_{pq} (p=1, 2, …, 5; q=1, 2, 3, …, 12) will be obtained. By applying these results in Eq. (24), the exact dynamic shape function of the structure can be rewritten (Eq. 27). By applying twelve boundary conditions on

The following connection is employed for nodal displacements and electrostatic potential on two edges of the element:

$$\begin{aligned}
\bar{N}_{xy1} &= \bar{N}_{xy}(x,0;\omega), \quad \bar{N}_{xy2} = \bar{N}_{xy}(x,b;\omega),\\
\bar{N}_{y1} &= \bar{N}_{y}(x,0;\omega), \quad \bar{N}_{y2} = \bar{N}_{y}(x,b;\omega),\\
\bar{M}_{xy1} &= \bar{M}_{xy}(x,0;\omega), \quad \bar{M}_{xy2} = \bar{M}_{xy}(x,b;\omega),\\
\bar{M}_{y1} &= \bar{M}_{y}(x,0;\omega), \quad \bar{M}_{y2} = \bar{M}_{y}(x,b;\omega),\\
\bar{Q}_{y1} &= \bar{Q}_{y}(x,0;\omega), \quad \bar{Q}_{y2} = \bar{Q}_{y}(x,b;\omega),\\
\bar{X}_{y1} &= \bar{X}_{y}(x,0;\omega), \quad \bar{X}_{y2} = \bar{X}_{y}(x,b;\omega),\\
X_y &= \int_{h}^{h+h_p} D_z(x,y,z,t)\,dz + \int_{-h-h_p}^{-h} D_z(x,y,z,t)\,dz
\end{aligned} \tag{31}$$

$$\{\bar{u}_{01} \quad \bar{v}_{01} \quad \bar{\psi}_{x1} \quad \bar{\psi}_{y1} \quad \bar{w}_1 \quad \bar{\varphi}_1 \quad \bar{u}_{02} \quad \bar{v}_{02} \quad \bar{\psi}_{x2} \quad \bar{\psi}_{y2} \quad \bar{w}_2 \quad \bar{\varphi}_2\}^T = H(\omega)c^T \tag{32}$$

where

$$H(\omega) = \begin{bmatrix}
1 & 1 & 1 & \dots & 1\\
r_{11} & r_{12} & r_{13} & \dots & r_{112}\\
r_{21} & r_{22} & r_{23} & \dots & r_{212}\\
r_{31} & r_{32} & r_{33} & \dots & r_{312}\\
r_{41} & r_{42} & r_{43} & \dots & r_{412}\\
r_{51} & r_{52} & r_{53} & \dots & r_{512}\\
e_1 & e_2 & e_3 & \dots & e_{12}\\
r_{11}e_1 & r_{12}e_2 & r_{13}e_3 & \dots & r_{112}e_{12}\\
r_{21}e_1 & r_{22}e_2 & r_{23}e_3 & \dots & r_{212}e_{12}\\
r_{31}e_1 & r_{32}e_2 & r_{33}e_3 & \dots & r_{312}e_{12}\\
r_{41}e_1 & r_{42}e_2 & r_{43}e_3 & \dots & r_{412}e_{12}\\
r_{51}e_1 & r_{52}e_2 & r_{53}e_3 & \dots & r_{512}e_{12}
\end{bmatrix} \tag{33}$$

In which $\hat{e}_1, \hat{e}_2, \hat{e}_3, \dots, \hat{e}_{12}$ are the components of the vector $\hat{e}(y,\omega)$. Furthermore, the following relation can be applied to the nodal force vector:

$$\{\bar{N}_{xy1} \quad \bar{N}_{y1} \quad \bar{M}_{xy1} \quad \bar{M}_{y1} \quad \bar{Q}_{y1} \quad \bar{X}_{y1} \quad \bar{N}_{xy2} \quad \bar{N}_{y2} \quad \bar{M}_{xy2} \quad \bar{M}_{y2} \quad \bar{Q}_{y2} \quad \bar{X}_{y2}\}^T = D(\omega)c^T \tag{34}$$

The matrix $D(\omega)$ components are defined in Appendix B. By eliminating the constant vector c from Eqs. (32) and (34) and connecting nodal force and nodal displacement vectors, the dynamic stiffness matrix can be expressed as:

$$[\bar{S}(\omega)] = [D(\omega)].[H(\omega)]^{-1} \tag{35}$$

In which $\bar{S}(\omega)$ is the elemental DSM. The Global DSM for the smart FG plate, which is called $\bar{S}_g(\omega)$, can be obtained by assembling the elemental DSM. It should be noted that, in the SEM, the assemblage process of the global system of equations is similar to the procedure of conventional FEM. In the frequency domain, the global displacement vector, d_g, and global force vector, f_g, are related by the global dynamic stiffness matrix:

$$\bar{S}_g(\omega)d_g = f_g \tag{36}$$

The spectral nodal displacement can be determined as:

$$d_g = S_g(\omega_n)^{-1} f_g \tag{37}$$

In Eq. (37), the nodal displacements are in the frequency domain, and by using the Inverse Fast Fourier Transform (IFFT), the time-domain nodal displacements can be generated. Finally, the fundamental natural frequency of the structure can be calculated by setting the determinant of the DSM equal to zero:

$$det\,\bar{S}_g(\omega_{NAT}) = 0 \tag{38}$$

3. Numerical results

Several examples are solved in this section to prove the exactness and efficiency of the presented method in free vibration and dynamic analysis of smart FG plates. In free vibration examples, only one or, in some cases, two spectral elements are utilized, and the results are confirmed by those obtained by other exact analytical methods. For dynamic analysis of smart isotropic and FG plates under different impact and moving loads, in order to apply the load in the middle of the plate and extract the transverse displacement of the middle point, two elements (for all kinds of boundary conditions) are employed and Abaqus software outputs validate the results. The mechanical and electrical properties of materials used in the following examples are tabulated in Table 1 (Farsangi et al. 2013). The material of the FG plate gradually varies through the thickness from the metal component (Ti-6Al-4V or Al) to the ceramic component (Aluminium Oxid or Al_2O_3).

Example 1

In this example, the accuracy and precision of the SEM in free and forced vibration analysis of square FG plates are investigated. In Table 2, the first three natural frequency parameters ($\hat{\omega} = \frac{\omega\pi^2 a^2}{h}\sqrt{\frac{\rho_m}{E_m}}$) of the FG plate (made of Al/Al_2O_3) with different power-law indices and various boundary conditions (which are a combination of Free (F), Simply supported (S), and Clamped (C) edges) are presented. Only one or two (for the SCSC boundary condition) elements are used in this example, and it can be observed from Table 2 that the results obtained by the SEM are in remarkable agreement with the Abaqus and analytical solutions. Also, the dynamic response of the SSSS FG plate under the action of an impact load, shown in Fig. 2, is depicted in Fig. 3, and obtained results are validated by those of the Abaqus simulation. For simulating the FG plate by Abaqus software, it is necessary to develop several partitions with different material properties through the plate thickness. Consequently, the plate is discretized by the solid element C3D8R. In order to achieve accurate results, at least 3 or 4 elements should be considered through the thickness of each partition, and accordingly, more elements are needed in the side directions to have a suitable element aspect ratio. As seen in Fig. 3, the Abaqus outputs (with 820000 elements and more than 14 hours run time with an i7 32GB Ram Desktop PC) are not exactly matched with those of the SEM. According to Fig. 3, the FE result's frequency and amplitude are higher and lower than the SEM results. According to Fig. 3, the FE result's frequency and amplitude are higher and lower than the SEM results. The FE result will be improved by increasing the number of elements in the thickness direction and consequently decreasing the structural stiffness, but this issue significantly increases the run time. Thus, in these examples, the results of the FG plate with Abaqus software are validated for perfect ceramic (n = 0) and metal (n = ∞) plates, which can be handled using shell element S4R. It should be noted that the

Application of the exact spectral element method in the analysis of the smart functionally graded plate

SEM accurate results, using only one or two elements, prove the proposed approach's efficiency in free and forced vibration analysis of FG plates.

Table 1 Material properties of plates and piezoelectric.

Property	Core plate				Piezoelectric layer	
	Ti-6Al-4V	Aluminium oxide	Al	Al_2O_3	G-1195 N	PZT-4
E (GPa)	105.7	320.24	70	380	63.0	-
υ	0.2981	0.2600	0.3	0.3	0.3	-
C_{11} (GPa)	-	-	-	-	-	132
C_{12} (GPa)	-	-	-	-	-	71
C_{33} (GPa)	-	-	-	-	-	115
C_{13} (GPa)	-	-	-	-	-	73
C_{55} (GPa)	-	-	-	-	-	26
e_{31} (cm^{-2})	-	-	-	-	44.37	-4.1
e_{33} (cm^{-2})	-	-	-	-	50.18	14.1
e_{15} (cm^{-2})	-	-	-	-	14.13	10.5
Ξ_{11} (nFm^{-1})	-	-	-	-	15.30	7.124
Ξ_{33} (nFm^{-1})	-	-	-	-	15.00	5.841
ρ (kgm^{-3})	4429	3750	2707	3800	7600	7500

Table 2 Three frequency parameters of square FG plate with different power law indices and boundary conditions (2h/a=0.01).

BCs.	n	Method	Mode numbers		
			1st	2nd	3rd
SCSC	0.5	Present	143.86 (1,1)	271.92 (1,2)	469.37 (2,2)
		Exact*	143.82	272.11	470.08
	2	Present	117.86 (1,1)	222.78 (1,2)	384.53 (2,2)
		Exact	117.81	222.81	385.07
SSSS	0.5	Present	98.13 (1,1)	245.21 (1,2)	392.14 (2,2)
		Exact	98.01	245.33	392.44
	2	Present	80.40 (1,1)	200.89 (1,2)	321.26 (2,2)
		Exact	80.35	200.88	321.41
SCSS	0.5	Present	117.53 (1,1)	256.74 (1,2)	427.63 (2,2)
		Exact	117.42	256.78	428.15
	2	Present	96.29 (1,1)	210.33 (1,2)	350.34 (2,2)
		Exact	96.27	210.39	350.71
SSSF	0.5	Present	58.06 (1,1)	137.79 (2,1)	293.16 (2,2)
		Exact	58.03	137.40	293.65
	2	Present	47.57 (1,1)	112.88 (2,1)	251.53 (2,2)
		Exact	47.55	112.96	251.92
SFSF	0.5	Present	47.88 (1,1)	80.06 (2,1)	182.09 (3,1)
		Exact	47.75	80.16	182.44
	2	Present	39.22 (1,1)	65.59 (2,1)	149.18 (3,1)
		Exact	39.17	65.64	149.06
SFSC	0.5	Present	63.03 (1,1)	164.09 (2,1)	312.64 (2,2)
		Exact	63.08	164.39	313.26
	2	Present	51.64 (1,1)	134.44 (2,1)	256.14 (2,2)
		Exact	51.63	134.70	256.58

*(Baferani et al. 2011)

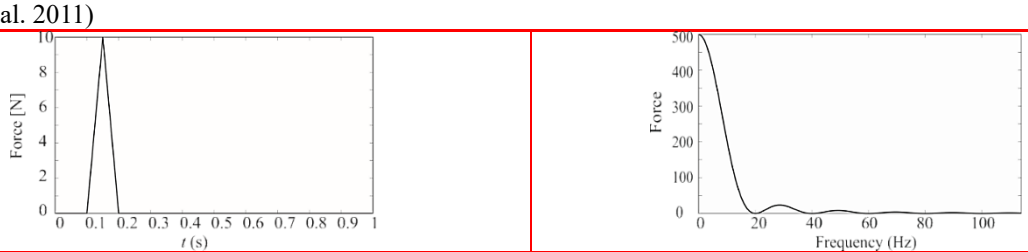

(a) Time domain (b) Frequency domain

Fig. 2 Triangular impact load in time and frequency domain

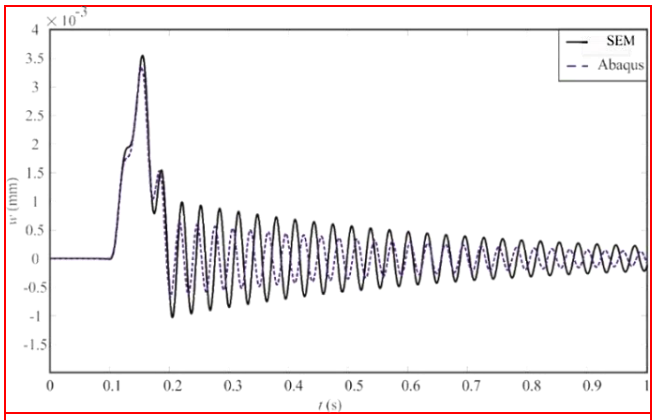

Fig. 3 Dynamic response of FG plate (n=1) under impact loading (a=2 m, 2h=0.02 m)

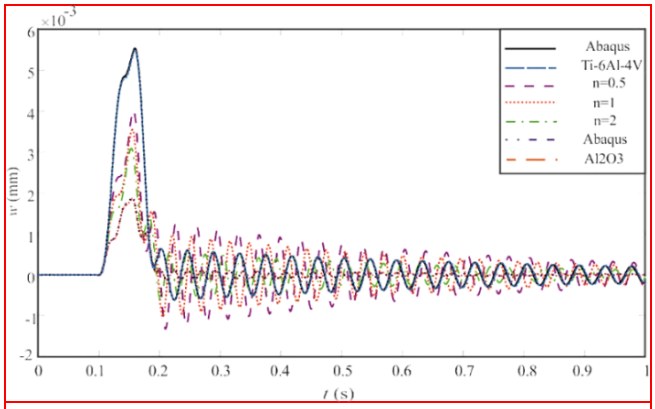

Fig. 4 Dynamic response of FG plate under impact loading (a=2 m, 2h=0.02 m)

Figure 4 shows the dynamic response of the SSSS FG plate with different power-law indices. As observed for two ceramic and metal plate limits, the SEM results are perfectly matched with the FE simulations. By changing the power-law index, the results vary between the margins of those of metal and ceramic.

Example 2

In this example, the exactness of the SEM in estimating the natural frequencies of the thin and thick FG plates (Al/Al_2O_3) integrated with two PZT-4 layers at the top and bottom faces is examined in Tables 3 and 4, respectively. It can be concluded from both tables that the smart FG plate with the higher thickness or more constraint has a higher natural frequency. According to the material properties listed in Table 1, by increasing n, the density and module of elasticity decrease and increase, respectively; consequently, increasing n decreases the natural frequency of the smart FG plates. Also, the Tables show that the percentage of errors in the SEM results compared with the analytical solution is less than 0.02%, proving the presented formulation's excellent accuracy.

The effect of the power-law index (n) on the dynamic response of the fully simply supported smart FG plate under impact loading is plotted in Fig. 5. It can be seen, by increasing n, the central deflection decreases, and in the case of n=0 (metal plate, Ti-6Al-4V), the dynamic response has the highest amplitude and lowest frequency. It should be mentioned that seven harmonic series (m=7) are used to reach a converged result. In Fig. 6, the transverse displacement of the above-mentioned smart FG plate (a=2 m, 2h=0.02 m, n=0.5) subjected to a triangular-shape impulsive load in the frequency domain is plotted, and the natural frequency of 73.2 Hz is distinguished in the figure.

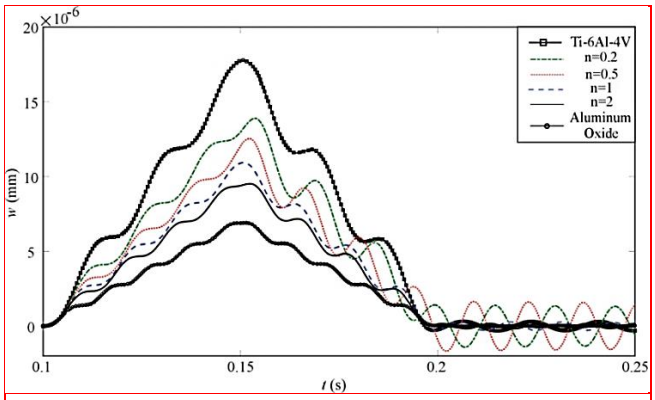

Fig. 5 Dynamic response of smart FG plate with different power law index under impact load

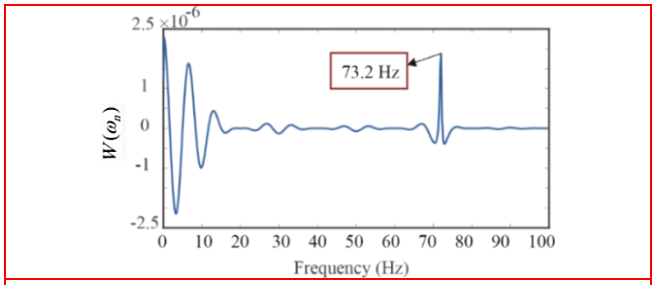

Fig. 6 The transverse displacement of the smart FG plate in the frequency domain

Example 3

This example shows the SE method's performance in calculating the natural frequencies of the different structures. Initially, the natural frequencies of the linearly varying (tapered) thickness smart plate are calculated. The plate is modelled as a stepped structure and divided into some rectangular strip elements with a constant thickness (as depicted in Fig. 7).

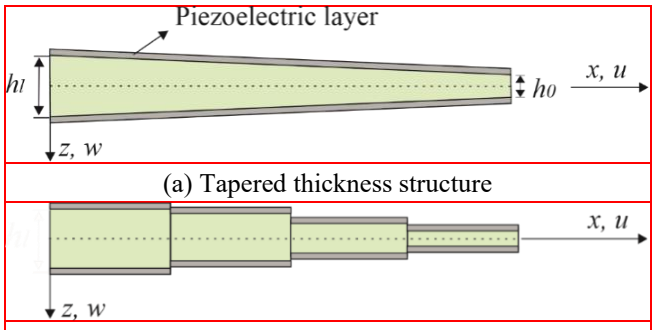

(a) Tapered thickness structure

(b) Elements with a constant thickness

Fig. 7 A schematic view of linearly variable thickness smart plate

The tapered ratio parameter is defined as follows (Mlzusawa 1993):

Application of the exact spectral element method in the analysis of the smart functionally graded plate

Table 3 Three natural frequencies (Hz) of square smart FG plate with different power law indices and boundary conditions (2h/a=0.05, h_p/2h=0.1).

BCs.	n	Method	Mode numbers		
			1st	2nd	3rd
SCSC	0.5	Present	533.535 (1,1)	997.945 (1,2)	1244.255 (2,2)
			[0.01]	[0.01]	[0.01]
		FSDT[1]	533.568	998.005	1244.321
	2	Present	458.109 (1,1)	856.114 (1,2)	1066.420 (2,2)
			[0.01]	[0.01]	[0.01]
		FSDT	458.149	856.189	1066.500
SSSS	0.5	Present	368.990 (1,1)	907.861 (1,2)	1430.553 (2,2)
			[0.01]	[0.01]	[0.01]
		RPT[2]	369.195 (1,1)	908.939 (1,2)	1433.121 (2,2)
			[0.05]	[0.11]	[0.17]
		FSDT	369.015	907.918	1430.642
	2	Present	317.104 (1,1)	779.552 (1,2)	1226.502 (2,2)
			[0.01]	[0.01]	[0.01]
		RPT	317.232 (1,1)	779.552 (1,2)	1227.01 (2,2)
			[0.03]	[0.03]	[0.03]
		FSDT	317.135	779.313	1226.615
SSSC	0.5	Present	439.418 (1,1)	947.150(2,1)	1066.675 (1,2)
			[0.01]	[0.01]	[0.01]
		FSDT	439.446	947.209	1066.737
	2	Present	377.488 (1,1)	812.788 (2,1)	914.927 (1,2)
			[0.01]	[0.01]	[0.01]
		FSDT	377.523	812.863	915.005
SSSF	0.5	Present	218.788 (1,1)	513.018 (1,2)	759.557 (2,1)
			[0.01]	[0.01]	[0.01]
		FSDT	218.802	513.044	759.598
	2	Present	188.128 (1,1)	440.681 (1,2)	652.209 (2,1)
			[0.01]	[0.01]	[0.01]
		FSDT	188.142	440.713	652.260
SFSF	0.5	Present	180.865 (1,1)	299.306 (1,2)	671.657 (1,3)
			[0.01]	[0.00]	[0.00]
		FSDT	180.881	299.312	671.687
	2	Present	155.532 (1,1)	257.305 (1,2)	576.598 (1,3)
			[0.01]	[0.00]	[0.01]
		FSDT	155.547	257.314	576.634
SFSC	0.5	Present	236.884 (1,1)	606.440 (1,2)	767.960 (2,1)
			[0.00]	[0.00]	[0.00]
		FSDT	236.898	606.470	767.999
	2	Present	203.667 (1,1)	520.657 (1,2)	659.394 (2,1)
			[0.01]	[0.01]	[0.01]
		FSDT	203.681	520.694	659.443

[percentage error] = (Present result – FSDT result) / (FSDT result) ×100

[1] (Askari Farsangi and Saidi 2012)

[2] (Rouzegar and Abad 2015)

$$\lambda = (h_1 - h_0)/h_0 \quad (39)$$

In Table 5, the first eight frequency parameters ($\bar{\omega} = \omega a^2\sqrt{\frac{\rho h_0}{D_0}}$) of an isotropic tapered square plate ($h_0 = 0.1, \lambda = 0.5$) are tabulated, and excellent agreement between the SEM results (with four strip elements) and other analytical solutions is evident.

Table 6 shows the convergence of both Abaqus and SEM results for the natural frequency of an Al_2O_3 plate (a=1 m, h_0=0.1 m, h_1=0.125 m, h_p=0.01 m) with two PZT-4 layers. Increasing the number of strip elements to more than four will not change the results, and the Abaqus results are converged with 14 elements in the thickness direction. Due to choosing just one element in the piezoelectric thickness direction, a 4.6% error is created; however, choosing more than one element in the piezoelectric thickness direction and considering an appropriate aspect ratio for elements lead to more than a million elements and a significant increase in the run time. Also, the first ten fundamental frequencies (Hz) of the above-mentioned smart plate are presented in Table 7. Since the structure is modelled differently in the SE method compared with Abaqus, some frequencies are missed.

Table 4 Three natural frequencies (Hz) of square smart FG plate with different power law indices and boundary conditions (2h/a=0.1, h_p/2h=0.1).

BCs.	*n*	Method	Mode numbers		
			1st	2nd	3rd
SCSC	0.5	Present	998.152 (1,1) [0.00]	1825.164 (1,2) [0.00]	2196.834 (2,2) [0.00]
		FSDT[1]	998.185	1825.231	2196.822
	2	Present	853.518 (1,1) [0.00]	1557.200 (1,2) [0.00]	1869.802 (2,2) [0.00]
		FSDT	853.554	1557.277	1869.767
SSSS	0.5	Present	715.276 (1,1) [0.01]	1691.876 (1,2) [0.01]	2579.954 (2,2) [0.01]
		RPT[2]	716.563 (1,1) [0.17]	1697.781 (1,2) [0.34]	2592.067 (2,2) [0.46]
		FSDT	715.319	1691.992	2580.078
	2	Present	613.249 (1,1) [0.01]	1445.016 (1,2) [0.02]	2197.674 (2,2) [0.01]
		RPT	613.982 (1,1) [0.11]	1446.529 (1,2) [0.08]	2199.028 (2,2) [0.05]
		FSDT	613.305	1445.353	2197.887
SSSC	0.5	Present	838.998 (1,1) [0.00]	1751.432 (2,1) [0.00]	1937.255 (1,2) [0.00]
		FSDT	839.040	1751.518	1937.295
	2	Present	718.485 (1,1) [0.01]	1495.324 (2,1) [0.01]	1651.902 (1,2) [0.00]
		FSDT	718.539	1495.435	1651.948
SSSF	0.5	Present	427.948 (1,1) [0.00]	976.397 (1,2) [0.00]	1426.794 (2,1) [0.00]
		FSDT	427.966	976.439	1426.860
	2	Present	367.386 (1,1) [0.01]	835.701 (1,2) [0.01]	1219.861 (2,1) [0.01]
		FSDT	367.407	835.753	1219.942
SFSF	0.5	Present	355.572 (1,1) [0.00]	577.402 (1,2) [0.00]	1255.975 (1,3) [0.00]
		FSDT	355.590	577.414	1256.026
	2	Present	305.373 (1,1) [0.01]	495.154 (1,2) [0.00]	1072.915 (1,3) [0.01]
		FSDT	305.394	495.169	1072.979
SFSC	0.5	Present	460.682 (1,1) [0.00]	1132.950 (1,2) [0.00]	1439.528 (2,1) [0.00]
		FSDT	460.698	1132.986	1439.591
	2	Present	395.327 (1,1) [0.00]	968.211 (1,2) [0.00]	1230.584 (2,1) [0.01]
		FSDT	395.346	968.255	1230.661

[percentage error] = (Present result – FSDT result) / (FSDT result) ×100
[1] (Farsangi and Saidi 2012)
[2] (Rouzegar and Abad 2015)

Furthermore, the natural frequencies of the FG plate (Al/Al_2O_3) with and without PZT-4 layers on an elastic foundation are calculated. Firstly, the frequency parameter ($\bar{\omega}$) of the FG plate rested on the elastic foundation ($\bar{K}_w = 100, \bar{K}_S = 10$) for different boundary conditions, aspect ratio and power-law indices are presented in Table 8.

Elastic foundation parameters are defined in Eq. (40), In which the $\bar{K}_S$ and $\bar{K}_W$ are Pasternak and Winkler parameters.

In Table 9, frequency parameters (ϖ) of the smart FG plate on the elastic foundation for different piezoelectric thicknesses and power-law indices are presented; and the SEM results are in excellent agreement with the analytical method based on refined plate theory (Rouzegar et al. 2015). For this part, elastic foundation parameters are defined as follows:

$$\bar{K}_S = \frac{K_S a^2}{A}, \bar{K}_W = \frac{K_W a^4}{A}, A = \frac{(2h)^3}{12(1-v^2)}\left[\frac{n(8+3n+n^2)E_m + 3(2+n+n^2)E_c}{(1+n)(2+n)(3+n)}\right]$$
$$\hat{\omega} = \omega h\sqrt{\rho_c/E_c} \quad (40)$$

Application of the exact spectral element method in the analysis of the smart functionally graded plate

$$K'_w = \frac{K_w b^4}{D_m}, K'_s = \frac{K_s b^2}{D_m}, D_m = E_m \frac{h^3}{12(1-\nu^2)}, \varpi = \omega h \sqrt{\frac{\rho_m}{E_m}} \quad (41)$$

Table 5 First eight frequency parameters ($\bar{\omega}$) of the tapered square plate.

Method	Mode number			
	1st	2nd	3rd	4th
SEM	31.70	57.77	68.24	90.52
Mizusawa (Mlzusawa 1993)	31.775	57.955	68.504	90.782
Manna (Manna 2006)	31.777	57.960	68.513	90.795
	Mode number			
	5th	6th	7th	8th
SEM	99.78	113.57	127.66	133.32
Mizusawa (Mlzusawa 1993)	100.25	114.37	127.80	133.80
Manna (Manna 2006)	100.27	114.40	-	-

Table 6 The natural frequency of the linearly tapered square smart plate.

Method	ω_1 (Hz)	Number of Elements
Abaqus 6*	864.05	112896
Abaqus 10	871.21	219024
Abaqus 14	872.61	352800
Abaqus 14	872.80	531380
SEM 2	864.2	2
SEM 3**	911.1	3
SEM 4	912.4	4
SEM 5	912.7	5
*Abaqus 6: 6 elements in the thickness direction **SEM 3: 3 sections		

Table 7 The first ten fundamental frequencies (Hz) of the smart plate

Method	Mode number				
	1st	2nd	3rd	4th	5th
SEM	912.7	2118.3	2175.3	-	-
Abaqus	872.80	2050.2	2113.0	2479.2	2479.8
	Mode number				
	6th	7th	8th	9th	10th
SEM	3189.2	3839.7	-	-	4754.8
Abaqus	3105.8	3808.3	3898.5	4114.2	4677.3

Example 4

As mentioned, performing the dynamic analysis of structures under moving loads with the least number of elements is another capability of the SEM. Figure 8 shows a smart plate subjected to a concentrated force (P) with constant speed (v) passing through the middle of the plate in the x-direction.

Table 8 Frequency parameter ($\hat{\omega}$) of the FG plate for different boundary conditions

a/b	n	Method	Boundary conditions				
			SSSF	SFSF	SCSF	SSSS	SSSC
0.5	0.25	SEM	0.1058	0.1037	0.1061	0.1184	0.12059
		FSDT[1]	0.1098	0.1060	0.1104	0.1184	0.1204
	1	SEM	0.0931	0.0914	0.0933	0.1038	0.1056
		FSDT	0.0978	0.0947	0.0982	0.1052	0.1066
	5	SEM	0.0820	0.0808	0.0822	0.0912	0.0927
		FSDT	0.0859	0.0834	0.0862	0.0922	0.0932
1	0.25	SEM	0.1097	0.1022	0.1125	0.1564	0.1713
		FSDT	0.1098	0.1061	0.1243	0.1559	0.1698
	1	SEM	0.0961	0.0901	0.9831	0.1358	0.1484
		FSDT	0.0978	0.0947	0.1095	0.1365	0.1448
	5	SEM	0.0841	0.0797	0.0861	0.1183	0.1286
		FSDT	0.0859	0.0834	0.0948	0.1179	0.1229
2	0.25	SEM	0.1226	0.1007	0.1482	0.301	0.3599
		FSDT	0.1545	0.1065	0.1803	0.2961	0.3426
	1	SEM	0.1059	0.0887	0.1271	0.2429	0.2926
		FSDT	0.1354	0.0948	0.1525	0.2467	0.2699
	5	SEM	0.0906	0.0784	0.1097	0.2206	0.2301
		FSDT	0.1160	0.0834	0.1271	0.2036	0.2150
[1] (Hosseini-Hashemi et al. 2010)							

Table 9 The frequency parameter (ϖ) of the FG plate with PZT-4 layers rested on the elastic foundation ($K'_W = 100, K'_S = 100$).

h_p/h	Theory	Power law index				
		0	0.5	1	2	5
10^{-1}	SEM	0.0360	0.0341	0.334	0.0329	0.0329
	RPT[1]	0.0360	0.0341	0.0333	0.0329	0.0328
10^{-2}	SEM	0.0404	0.0386	0.0377	0.0374	0.0376
	RPT	0.0404	0.0385	0.0377	0.0373	0.0376
10^{-4}	SEM	0.0410	0.0393	0.0384	0.0381	0.0384
	RPT	0.0411	0.0392	0.0384	0.0381	0.0383
[1] (Rouzegar et al. 2015)						

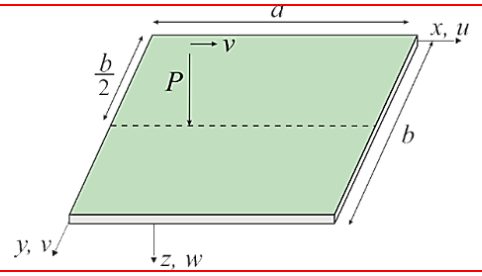

Fig. 8 The smart plate subjected to the moving load.

Equation (42) describes the applied moving load:

$$f_m(y,t) = \frac{2P}{a} sin(\frac{m\pi}{a} vt) \qquad a = vt_e \tag{42}$$

In which t_e is the effective time (the time that the applied load needs to pass over the plate length). It can be observed in Fig. 9 that five harmonic series are sufficient to have converged results for the smart isotropic plate subjected to a moving load with P=10 kN and v=25 m/s. Also, this figure verifies the exactness of SEM results by finite element analysis (with ten elements through the plate thickness).

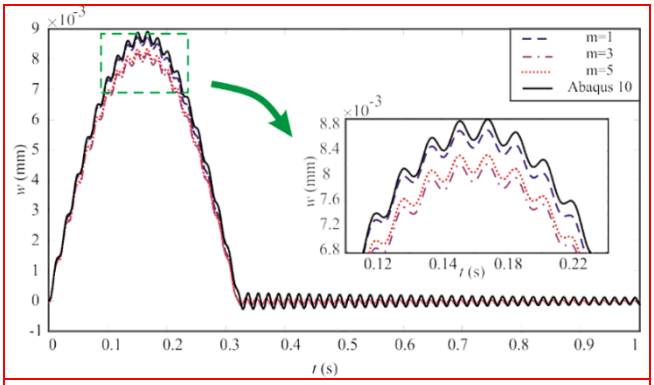

Fig. 9 The effect of the number of harmonic series on the dynamic response of the smart isotropic plate with SSSS boundary condition.

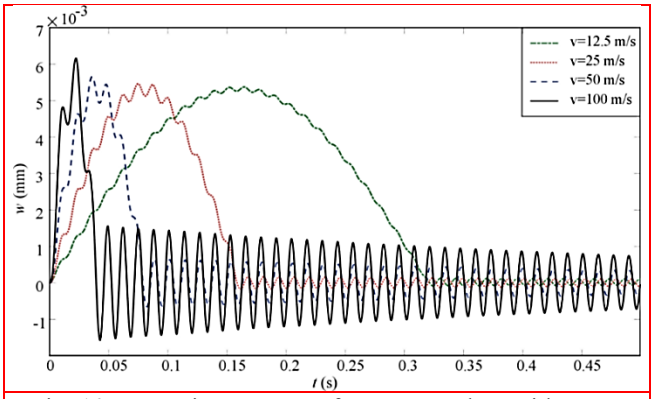

Fig. 10 Dynamic response of smart FG plate with SSSS boundary condition under moving load.

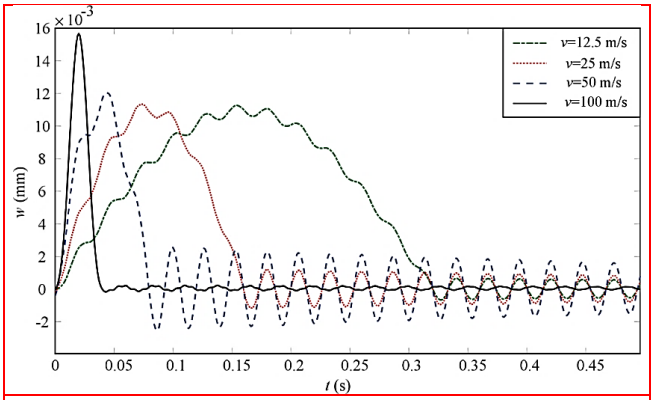

Fig. 11 Dynamic response of smart FG plate with SFSF boundary condition under moving load.

The dynamic response of the smart FG plate (n=1) subjected to moving loads (P=10 kN) with different velocities and boundary conditions of SSSS and SFSF are plotted in Figs. 10 and 11. These figures indicate that, although a loading with higher speed has less effective time (t_e), it leads to higher central deflection, an exciting conclusion, especially for energy harvesting studies. Also, the fully supported smart FG plate has less central deflection compared with the structure with SFSF boundary conditions due to more constraints.

In Fig. 12, the effect of different boundary conditions on the dynamic response of the smart FG plate (n=1) subjected to moving load (P=10 kN, v=12.5 m/s) is studied. As expected, the plates with more constraints have higher stiffness, and consequently, the plate with SCSC and SFSF boundary conditions has the lowest and highest central deflection, respectively.

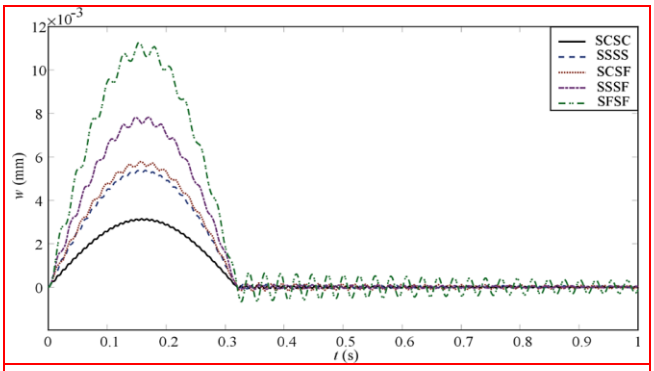

Fig. 12 The effect of boundary conditions on the dynamic response of the smart FG plate.

Also, the effect of the power-law index on the dynamic response of the fully simply supported smart FG plate under a moving load (P=10 kN, v=25 m/s) is shown in Fig. 13. As discussed before, by increasing n, the density and module of elasticity of the smart FG plate are decreased and increased, respectively, and in the case of fully metal substrate (Ti-6Al-4V), the dynamic response has the highest amplitude and lowest frequency. Furthermore, the dynamic response of fully simply supported smart FG and isotropic plate under the action of the moving load for different piezoelectric thicknesses are plotted in Figs. 14(a)-(b). It can be observed that because of the higher stiffness of the structure, the response amplitude is decreased by increasing piezoelectric thickness.

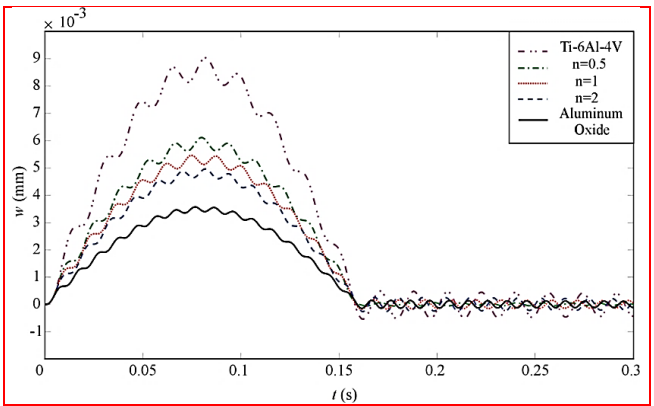

Fig. 13 Dynamic response of the smart FG plate with different power law indices subjected to moving load.

Application of the exact spectral element method in the analysis of the smart functionally graded plate

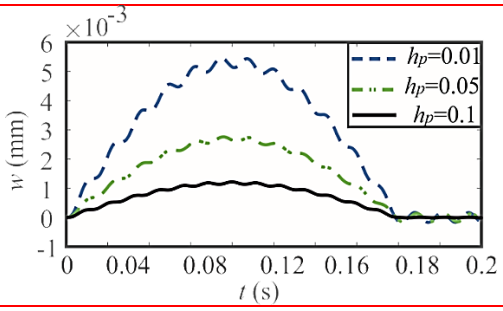

(a) Smart FG plate (n=1)

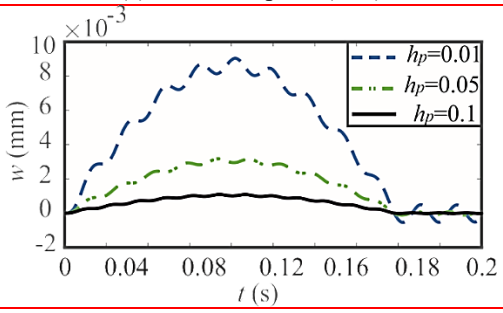

(b) Smart isotropic plate

Fig. 14 The effect of piezoelectric thickness on the dynamic response of the smart FG and isotropic plate under moving load (P=10 kN, v=25 m/s).

4. Conclusion

This study extends the exact spectral element method (SEM) for wave propagation analysis of FG and isotropic plates integrated with two piezoelectric layers on their surfaces. Differential equations of motion are derived using the Mindlin plate theory assumption, Hamilton's principle, and Maxwell's equation. The structure's dynamic stiffness matrix (DSM) is formed by applying a closed-form solution for a Levy-type smart FG plate and some algebraic manipulation. Several free and forced vibration and dynamic problems are solved, and existing solutions and finite element analyses validate the accuracy and precision of the results. The main conclusions are as follows:

- Free and forced vibration analyses of isotropic and FG plates are performed, and the obtained results are in excellent agreement with the exact method and Abaqus software.
- Natural frequencies of thick and thin FG plates with two PZT-4 layers are calculated and the maximum percentage error compared with existing exact solutions is less than 0.02%, which proves the accuracy of the presented method.
- The wave propagation in smart isotropic and FG plates under the action of impact and moving loads is examined, and the effects of various parameters on the results are studied, too.
- The effect of moving load with different speeds on the dynamic response of smart FG plates is investigated, and it is deduced that less effective time leads to higher central deflection.
- The effects of boundary condition, power-law index, and piezoelectric thickness on the dynamic response of the smart isotropic and FG plates under impact and moving loads are studied, and logical results are observed.

Declaration of Competing Interest

The authors declare that they have no known competing financial interests or personal relationships that could have appeared to influence the work reported in this paper.

Availability of data and material

The data presented in this study are available on request from the corresponding author. The data are not publicly available because it forms part of an ongoing study.

Appendix A

Coefficients in Eq. (4) are introduced as:

$$\bar{C}_{11} = C_{11} - \frac{{C_{13}}^2}{C_{33}}, \bar{C}_{12} = C_{12} - \frac{{C_{13}}^2}{C_{33}},$$
$$\bar{e}_{31} = e_{31} - \frac{C_{13}}{C_{33}} e_{33}, \bar{\Xi}_{33} = \Xi_{33} + \frac{{e_{33}}^2}{C_{33}} \quad \text{(A1)}$$

Also, coefficients in Eq. (18) are presented as:

$$(A_{11}, A_{12}) = \int_{-h}^{h} (Q_{11}, Q_{12}) dz + 2\int_{h}^{h+h_p} (C_{11}, C_{12}) dz,$$
$$A_{66} = \int_{-h}^{h} Q_{66} dz + \int_{h}^{h+h_p} (C_{11} - C_{12}) dz,$$
$$A_{55} = \int_{-h}^{h} \kappa^2 Q_{66} dz + 2\int_{h}^{h+h_p} \kappa^2 C_{55} dz,$$
$$(B_{11}, B_{12}) = \int_{-h}^{h} (Q_{11}, Q_{12}) z dz + 2\int_{h}^{h+h_p} (C_{11}, C_{12}) z dz,$$
$$B_{66} = \int_{-h}^{h} Q_{66} z dz + \int_{h}^{h+h_p} (C_{11} - C_{12}) z dz,$$
$$(F_{11}, F_{12}) = \int_{-h}^{h} (Q_{11}, Q_{12}) z^2 dz + 2\int_{h}^{h+h_p} (C_{11}, C_{12}) z^2 dz,$$
$$F_{66} = \int_{-h}^{h} Q_{66} z^2 dz + \int_{h}^{h+h_p} (C_{11} - C_{12}) z^2 dz \quad \text{(A2)}$$

and

$$\lambda_1 = -\frac{4}{3}\bar{e}_{31} h_p, \lambda_2 = -\frac{8}{9}\Xi_{11} h_p, \lambda_3 = \frac{4}{3} e_{15} h_p,$$
$$\lambda_4 = \frac{4}{3} h_p (\bar{e}_{31} + e_{15}), \lambda_5 = \frac{32\bar{\Xi}_{33}}{3h_p},$$
$$\lambda_0 = \frac{4}{3} h_p \quad \text{(A3)}$$

Appendix B

The z_{ij} coefficients in Eq. (25) are as below:

$$z_{11}=-A_{11}\left(\frac{m\pi}{a}\right)^2-A_{66}k^2+I_0\omega^2, z_{12}=-z_{21}=-i(A_{11}-A_{66})\left(\frac{m\pi}{a}\right)k,$$
$$z_{13}=z_{31}=-B_{11}\left(\frac{m\pi}{a}\right)^2-B_{66}k^2+I_1\omega^2, z_{14}=-z_{41}=-i(B_{11}-B_{66})\left(\frac{m\pi}{a}\right)k,$$
$$z_{15}=z_{51}=z_{16}=z_{61}=0, z_{22}=-A_{11}k^2-A_{66}\left(\frac{m\pi}{a}\right)^2+I_0\omega^2,$$
$$z_{23}=-z_{32}=i(B_{11}-B_{66})\left(\frac{m\pi}{a}\right)k, z_{24}=z_{42}=-B_{11}k^2-B_{66}\left(\frac{m\pi}{a}\right)^2+I_1\omega^2,$$
$$z_{25}=z_{52}=z_{26}=z_{62}=0, z_{33}=-F_{11}\left(\frac{m\pi}{a}\right)^2-F_{66}k^2-A_{55}+(I_2-ic_0)\omega^2,$$
$$z_{34}=-z_{43}=-i(F_{11}-F_{66})\left(\frac{m\pi}{a}\right)k, z_{35}=z_{53}=-A_{55}\left(\frac{m\pi}{a}\right), z_{36}=(\lambda_2-\lambda_1)\left(\frac{m\pi}{a}\right),$$
$$z_{44}=-F_{11}k^2-F_{66}\left(\frac{m\pi}{a}\right)^2-A_{55}+(I_2-ic_0)\omega^2, z_{45}=-z_{54}=iA_{55}k, z_{46}=ik(\lambda_1-\lambda_2),$$
$$z_{55}=-A_{55}\left(\left(\frac{m\pi}{a}\right)^2+k^2\right)+(I_0-ic_0)\omega^2, z_{56}=\lambda_2\left(\left(\frac{m\pi}{a}\right)^2+k^2\right), z_{63}=-(\lambda_2+\lambda_1)\left(\frac{m\pi}{a}\right),$$
$$z_{64}=-i(\lambda_2+\lambda_1)k, z_{65}=-\lambda_2\left(\left(\frac{m\pi}{a}\right)^2+k^2\right), z_{66}=\lambda_2\left(\left(\frac{m\pi}{a}\right)^2+k^2\right)+\lambda_4 \quad \text{(B1)}$$

Also, the components of matrix $D(\omega)$ in Eq. (33) are defined as below:

$$[D_{1j}]=\left[A_{66}\left(ik_j-\left(\frac{m\pi}{a}\right)r_{1j}\right)+B_{66}\left(ik_jr_{2j}-\left(\frac{m\pi}{a}\right)r_{3j}\right)\right],$$
$$[D_{2j}]=\left[iA_{11}k_jr_{1j}+A_{12}\left(\frac{m\pi}{a}\right)+iB_{11}k_jr_{3j}+B_{12}\left(\frac{m\pi}{a}\right)r_{2j}\right],$$
$$[D_{3j}]=\left[B_{66}\left(ik_j-\left(\frac{m\pi}{a}\right)r_{1j}\right)+F_{66}\left(ik_jr_{2j}-\left(\frac{m\pi}{a}\right)r_{3j}\right)\right],$$
$$[D_{4j}]=\left[iB_{11}k_jr_{1j}+B_{12}\left(\frac{m\pi}{a}\right)+iF_{11}k_jr_{3j}+F_{12}\left(\frac{m\pi}{a}\right)r_{2j}-\lambda_1r_{5j}\right],$$
$$[D_{5j}]=\left[A_{55}(ik_jr_{4j}-r_{3j})-\lambda_2(ik_jr_{5j})\right],$$
$$[D_{6j}]=\left[2h_pe_{51}(r_{3j}-ik_jr_{4j})-\Xi_{11}(ik_jr_{5j})\lambda_0\right],$$
$$[D_{7j}]=\left[A_{66}\left(ik_j-\left(\frac{m\pi}{a}\right)r_{1j}\right)+B_{66}\left(ik_jr_{2j}-\left(\frac{m\pi}{a}\right)r_{3j}\right)\right]exp(-ik_jb),$$
$$[D_{8j}]=\left[iA_{11}k_jr_{1j}+A_{12}\left(\frac{m\pi}{a}\right)+iB_{11}k_jr_{3j}+B_{12}\left(\frac{m\pi}{a}\right)r_{2j}\right]exp(-ik_jb),$$
$$[D_{9j}]=\left[B_{66}\left(ik_j-\left(\frac{m\pi}{a}\right)r_{1j}\right)+F_{66}\left(ik_jr_{2j}-\left(\frac{m\pi}{a}\right)r_{3j}\right)\right]exp(-ik_jb),$$
$$[D_{10j}]=\left[iB_{11}k_jr_{1j}+B_{12}\left(\frac{m\pi}{a}\right)+iF_{11}k_jr_{3j}+F_{12}\left(\frac{m\pi}{a}\right)r_{2j}-\lambda_1r_{5j}\right]exp(-ik_jb),$$
$$[D_{11j}]=\left[A_{55}(ik_jr_{4j}-r_{3j})-\lambda_2(ik_jr_{5j})\right]exp(-ik_jb),$$
$$[D_{12j}]=\left[2h_pe_{51}(r_{3j}-ik_jr_{4j})-\Xi_{11}(ik_jr_{5j})\lambda_0\right]exp(-ik_jb), \quad \text{(B2)}$$

References

Abad, F. and Rouzegar, J. (2017), "An exact spectral element method for free vibration analysis of FG plate integrated with piezoelectric layers", Composite Structures. **180** 696-708.

Abad, F. and Rouzegar, J. (2019), "Exact wave propagation analysis of moderately thick Levy-type plate with piezoelectric layers using spectral element method", *Thin-Walled Structures*. **141** 319-331.

Abbaspour, F. and Arvin, H. (2021), "Thermo-electro-mechanical buckling analysis of sandwich nanocomposite microplates reinforced with graphene platelets integrated with piezoelectric facesheets resting on elastic foundation", *Computers & Mathematics with Applications*. **101** 38-50.

Ahmed, R.A., Khalaf, B.S., Raheef, K.M., Fenjan, R.M. and Faleh, N.M. (2021), "Investigating dynamic response of nonlocal functionally graded porous piezoelectric plates in thermal environment", *Steel Compos. Struct*. **40**(2), 243-254.

Al-Osta, M.A. (2022), "Wave propagation investigation of a porous sandwich FG plate under hygrothermal environments via a new first-order shear deformation theory", *Steel and Composite Structures*. **43**(1), 117-127.

Askari Farsangi, MA and Saidi, A.R. (2012), "Levy type solution for free vibration analysis of functionally graded rectangular plates with piezoelectric layers", *Smart Mater Struct*. **21**(9), 094017.

Azandariani, M.G., Gholami, M. and Zare, E. (2022), "Development of spectral element method for free vibration of axially-loaded functionally-graded beams using the first-order shear deformation theory", *European Journal of Mechanics - A/Solids*. 104759.

Baferani, A.H., Saidi, A. and Jomehzadeh, E. (2011), "An exact solution for free vibration of thin functionally graded rectangular plates", *Proceedings of the Institution of Mechanical Engineers, Part C: Journal of Mechanical Engineering Science*. **225**(3), 526-536.

Application of the exact spectral element method in the analysis of the smart functionally graded plate

Ebrahimi, F. and Barati, M.R. (2016), "A nonlocal higher-order refined magneto-electro-viscoelastic beam model for dynamic analysis of smart nanostructures", *International Journal of Engineering Science*. **107** 183-196.

Ebrahimi, F. and Barati, M.R. (2018), "Vibration analysis of smart piezoelectrically actuated nanobeams subjected to magneto-electrical field in thermal environment", *Journal of Vibration and Control*. **24**(3), 549-564.

Farsangi, M.A. and Saidi, A. (2012), "Levy type solution for free vibration analysis of functionally graded rectangular plates with piezoelectric layers", *Smart Mater Struct*. **21**(9), 094017.

Farsangi, M.A., Saidi, A. and Batra, R. (2013), "Analytical solution for free vibrations of moderately thick hybrid piezoelectric laminated plates", *Journal of Sound and Vibration*. **332**(22), 5981-5998.

Fazeli, S., Stokes-Griffin, C., Gilbert, J. and Compston, P. (2021), "An analytical solution for the vibrational response of stepped smart cross-ply laminated composite beams with experimental validation", *Composite Structures*. **266** 113823.

Fenjan, R.M., Ahmed, R.A. and Faleh, N.M. (2021), "Post-buckling analysis of imperfect nonlocal piezoelectric beams under magnetic field and thermal loading", *Struct. Eng. Mech*. **78**(1), 15-22.

Fenjan, R.M., Ahmed, R.A., Faleh, N.M. and Hani, FM (2020), "Static stability analysis of smart nonlocal thermo-piezo-magnetic plates via a quasi-3D formulation", *Smart Struct. Syst*. **26**(1), 77-87.

Hosseini-Hashemi, S., Taher, H.R.D., Akhavan, H. and Omidi, M. (2010), "Free vibration of functionally graded rectangular plates using first-order shear deformation plate theory", *Applied Mathematical Modelling*. **34**(5), 1276-1291.

Jiang, W.-W., Gao, X.-W., Xu, B.-B. and Lv, J. (2021), "Analysis of piezoelectric problems using zonal free element method", *Engineering Analysis with Boundary Elements*. **127** 40-52.

Joglekar, D.M. and Mitra, M. (2016), "Analysis of flexural wave propagation through beams with a breathing crack using wavelet spectral finite element method", *Mechanical Systems and Signal Processing*. **76** 576-591.

Khalili, A., Jha, R. and Samaratunga, D. (2017), "The Wavelet Spectral Finite Element-based user-defined element in Abaqus for wave propagation in one-dimensional composite structures", *Simulation*. **93**(5), 397-408.

Koizumi, M. (1993), "The concept of FGM", *Ceramic transactions*. **34** 3-10.

Kulkarni, H., Zohaib, K., Khusru, A. and Shravan Aiyappa, K. (2018), "Application of piezoelectric technology in automotive systems", *Materials Today: Proceedings*. **5**(10, Part 1), 21299-21304.

Kulkarni, R.B., Gopalakrishnan, S. and Trikha, M. (2022), "Material property identification in composite structures using time domain spectral elements", *Composite Structures*. **292** 115656.

Lee, U. (2009), *Spectral element method in structural dynamics*, John Wiley & Sons

Liu, C., Yu, J., Zhang, B., Zhang, X. and Elmaimouni, L. (2021), "Analysis of Lamb wave propagation in a functionally graded piezoelectric small-scale plate based on the modified couple stress theory", *Composite Structures*. **265** 113733.

Liu, J., Zhang, X., Wang, J., Gu, L., Chu, P.K. and Yu, X.-F. (2022), "Global structure search for new 2D PtSSe allotropes and their potential for thermoelectirc and piezoelectric applications", *Chemical Physics Letters*. **805** 139913.

Liu, X. (2016), "Spectral dynamic stiffness formulation for inplane modal analysis of composite plate assemblies and prismatic solids with arbitrary classical/nonclassical boundary conditions", *Composite Structures*. **158** 262-280.

Liu, X., Kassem, H. and Banerjee, J. (2016), "An exact spectral dynamic stiffness theory for composite plate-like structures with arbitrary non-uniform elastic supports, mass attachments and coupling constraints", *Composite Structures*. **142** 140-154.

Lv, J., Shao, M., Cui, M. and Gao, X. (2019), "An efficient collocation approach for piezoelectric problems based on the element differential method", *Composite Structures*. **230** 111483.

Manna, M. (2006), "A sub-parametric shear deformable element for free vibration analysis of thick/thin rectangular plates with tapered thickness", *Applied Mechanics and Engineering*. **11**(4), 901.

Martínez-Ayuso, G., Friswell, M.I., Khodaparast, H.H., Roscow, JI and Bowen, C.R. (2019), "Electric field distribution in porous piezoelectric materials during polarization", *Acta Materialia*. **173** 332-341.

Mirjavadi, S.S., Forsat, M., Barati, M.R. and Hamouda, A.S. (2022), "Geometrically nonlinear vibration analysis of eccentrically stiffened porous functionally graded annular spherical shell segments", *Mechanics Based Design of Structures and Machines*. **50**(6), 2206-2220.

Mlzusawa, T. (1993), "Vibration of rectangular Mindlin plates with tapered thickness by the spline strip method", *Computers & structures*. **46**(3), 451-463.

Mokhtari, A., Mirdamadi, H.R. and Ghayour, M. (2017), "Wavelet-based spectral finite element dynamic analysis for an axially moving Timoshenko beam", *Mechanical Systems and Signal Processing*. **92** 124-145.

Nanda, N. and Kapuria, S. (2015), "Spectral finite element for wave propagation analysis of laminated composite curved beams using classical and first order shear deformation theories", *Composite Structures*. **132** 310-320.

Narayanan, G. and Beskos, D. (1978), "Use of dynamic influence coefficients in forced vibration problems with the aid of fast Fourier transform", *Computers & Structures*. **9**(2), 145-150.

Newland, D.E. (2012), *An introduction to random vibrations, spectral & wavelet analysis*, Courier Corporation

Panda, S., Hajra, S., Mistewicz, K., In-na, P., Sahu, M., Rajaitha, P.M. and Kim, H.J. (2022), "Piezoelectric energy harvesting systems for biomedical applications", *Nano Energy*. **100** 107514.

Rouzegar, J. and Abad, F. (2015), "Free vibration analysis of FG plate with piezoelectric layers using four-variable refined plate theory", *Thin-Walled Structures*. **89** 76-83.

Rouzegar, J., Lotfavar, A. and Abad, F. (2015), "Free vibration analysis of FG plate with piezoelectric layers on elastic foundation using refined shear deformation theory", *The 23rd Annual International Conference on Mechanical Engineering-ISME2015.* Tehran, May.

Shirmohammadi, F., Bahrami, S., Saadatpour, M.M. and Esmaeily, A. (2015), "Modeling wave propagation in moderately thick rectangular plates using the spectral element method", *Applied Mathematical Modelling*. **39**(12), 3481-3495.

Szilard, R. (2004), "Theories and applications of plate analysis: classical, numerical and engineering methods", *Appl. Mech. Rev.*, **57**(6), B32-B33.

Taherifar, R., Zareei, S.A., Bidgoli, M.R. and Kolahchi, R. (2020), "Seismic analysis in pad concrete foundation reinforced by nanoparticles covered by smart layer utilizing plate higher order theory", *Steel and Composite Structures, An International Journal*. **37**(1), 99-115.

Tran, H.-Q., Vu, V.-T. and Tran, M.-T. (2023), "Free vibration analysis of piezoelectric functionally graded porous plates with graphene platelets reinforcement by pb-2 Ritz method", *Composite Structures*. **305** 116535.